Aalto University

Gong, Jing hu; Wang, Jun; Lund, Peter D.; Zhao, Dan dan; Xu, Jing wen; Jin, Yi hao

Comparative study of heat transfer enhancement using different fins in semi-circular absorber tube for large-aperture trough solar concentrator

Comparative study of heat transfer enhancement using different fins in semi-circular absorber tube for large-aperture trough solar concentrator

Jing-hu Gong[1,2], Jun Wang[1,2,*], Peter D. Lund[1,3,*], Dan-dan Zhao[1,2], Jing-wen Xu[1,2], Yi-hao Jin[1,2]

[1] Key Laboratory of Solar Energy Science and Technology in Jiangsu Province, Southeast University, Nanjing 210096, China

[2] School of Energy and Environment, Southeast University, Nanjing 210096, China

[3] School of Science, Aalto University, FI-00076 Aalto (Espoo), Finland

First author: gongjinghu0103@163.com (JH. Gong)

*Corresponding authors: 101010980@seu.edu.cn (J. Wang); peter.lund@aalto.fi (P. D. Lund)

Abstract

An improved evacuated absorber tube (AT) design consisting of a semi-circular tube is proposed for large-aperture parabolic trough concentrator. The absorber tube also contains a flat-plate radiation shield in the vacuum part of the tube in the glass cover. To enhance the heat transfer in the AT, different fins geometries added to the bottom of the AT were analyzed here. Compared to an AT without fins, the thermal efficiency of the tube could be increased from 75.7% to 76.9% with a short and thick fin and to 77.3% with a long and thin fin in the flow velocity range of 0.4-1.5m/s. The long and thin finned AT shows better enhancement of heat transfer, but the heat transfer performance factor also accounting for frictional losses is higher for short and thick fin. Simultaneously, increasing the number of long and thin fins in the AT would not improve much the heat transfer performance.

Keywords: large-aperture parabolic trough concentrator; semi-circular absorber tube; flat-plate radiation shield; fin; heat transfer

Nomenclature

Symbols

C_1, C_2, C_u	Constants for the realizable k-ε turbulence model
C_p	The specific heat capacity of HTF, J/(kg K)
DNI	Direct normal irradiance, W/m^2
D_{gla}	Diameter of the glass cover, m
D_{ri}	Inner diameter of absorber tube, m
E	Heat flux, W/m^2
f	Friction factor, -
G_k	Generation of turbulent kinetic energy due to mean velocity gradients, kg/m s^3
g	Gravity acceleration, m/s^2
H	Thickness of collector tube, mm
h_f	Convection heat transfer coefficient, W/m^2 K
h	Distance form plat-plate radiation shield to plane part of AT, mm
K	Width of flat-plate radiation shield, mm
K_f	Thermal conductivity of HTF, W/m K
L	Length, mm
M	Primary reflector aperture width, m
Nu	Nusselt number
∇P	Pressure drop, Pa
Pr	Prandtl number, -
q	The heat flux density at the inner surface, W/m^2
Q_u, Q_{loss}	Heat absorbed and lost, W
R	Radius of the absorber tube, m
T	Temperature, K
t	Time, s
U	velocity vector of HTF
u, v, w	x, y, z velocity components, m /s
i, j, k	Cartesian coordinates

Greek letters

α	Thermal diffusion coefficient
ε_{abs}	Emissivity, %
η_{opt}, η_{th}	Optical and thermal efficiency, %

φ	Half rim angle, degs
ρ_r	Reflectance of collector mirror, %
ρ	Density, kg/m^3
υ	Coefficient of dynamic viscosity of HTF, m Pa s
σ_k, σ_ε	Prandtl number for transport of turbulent dissipation rate, ε/k
σ_T	Prandtl number for energy, -
σ_{spec}	Mirror specularity error, mrad
τ_{gla}	Transmissivity of the glass cover, %
ζ_{abs}	Absorptance of the selective coating, %

Subscripts

abs	absorber
ave	average
gla	glass cover
max	maximum
min	minimum
opt	optical
th	thermal
U	useful

Abbreviations

AT	Absorber tube
CSP	Concentrating solar power
HTF	Heat transfer fluid
PR	Primary reflector
SR	Secondary reflector

32

1. Introduction

34

35 Concentrating solar power (CSP) is considered a potential solar energy technology [1-3]. CSP can be

realized through a parabolic trough, linear Fresnel, solar tower and parabolic dish [2-4]. The trough is basically the only commercial CSP technology accounting for 90% of the CSP market [1, 5, 6]. However, the trough CSP is still more expensive than traditional thermal power [5-10]. Reducing the cost and improving the competitiveness of the trough technology is therefore highly relevant [7, 8]. A large-aperture trough concentrator can reduce the use of auxiliary components and thereby also reduce the costs [5-10]. In addition, such as system can reach a higher efficiency and performance when using a high temperature heat transfer fluid (HTF) and absorber tube (AT) [5-10]. The state-of-the-art of large-aperture systems include the 8.2m Space Tube® by Abengoa [6], 6.87m SENER trough®-2 by Sener [6], 7-9 m Sky Trough by Sky Fuel, and the 7.51 m Ultimate Trough by Flabeg [6, 9, 10]. The Ultimate Trough has demonstrated cost reductions through increased aperture size trough [9, 10]. Some of these systems are commercially available.

Typically, a large-aperture collector is equipped with a large-diameter AT to increase the intercept factor [5-8]. However, a larger diameter means also a larger surface area resulting in higher heat losses [6]. Often the radiation losses are suppressed and the intercept factor is increased by using a smaller diameter AT and matching with a secondary reflector (SR), e.g. a Compound Parabolic Concentrator (CPC) [11, 12], flat plate mirror [13], multi-surface concentrator [14, 15] or a SR designed by adaptive method [5]. To improve the interception factor, reduce the cosine loss, multiple reflection losses and the external radiation area, the state-of-the-art of a semi-circular AT with a reflector and outer fins is designed and researched in an 8m width aperture trough concentrator. An optical and thermal efficiency above 80% could be possible with the last-mentioned approach for a large-aperture trough solar concentrator system [6].

The heat transfer enhancement in the absorber tube is of importance to the overall performance of the concentrator [7, 8], as it would improve the thermal efficiency, avoid local overheating and damaging the absorber coating, and reducing thermal stresses and bending to protect the collector tube from being damaged [4, 7, 8]. The heat transfer enhancement can be achieved through the following means [7]: Inserting a vortex generator inside the HTF [7] such as a twisted tape [16], wavy-tape [17], wire coil [18], screw-tap [19], star flow tape [20], metal foam [21], array perforated plate [22], internal multiple-fin array [23], etc., which would better mix the heat transfer fluid to form the secondary flow and enhance the heat transfer [4, 8]. Secondly, the geometric shape of the AT inner wall [8] could be changed, e.g. a longitudinal vortex generator [24], fins [25-28], outward convex corrugated [29, 30] or a dimple [31] could be installed on the inner wall of the AT to create turbulent flow conditions. The solid-liquid heat transfer contact area is increased and simultaneously the direction of the flow

could also is changed to form a secondary flow [8, 32]. Thirdly adding nano-particles along with or without magnetic field into the HTF to form nano-fluids such as Al_2O_3, Fe_3O_4, Cu, CuO, Al, TiO_2, SiO_2, ZnO, Au, SiC, CNT, etc. [33-37] would increase the thermal conductivity of the HTF and improve the heat transfer [8]. The thermal efficiency can be increased up to 2%-2.5% by traditional heat transfer enhancement approaches, but also leading to a higher friction and pumping power consumption [8, 38].

Inserting a vortex generator inside the HTF is simple to manufacture, but the resulting heat transfer improvement is modest and the pumping power increase is high [8]. The pump consumption (friction) of nano-fluids is also high, nanoparticles are expensive, and some could even be toxic [8]. Absorber tubes with fins and dimple in the inner wall of the AT are the most promising approach with a high enhanced heat transfer rate, but low pumping power consumption (friction) [8, 39, 40]. The advantage of a dimple tube is the increase the solid-liquid interface surface, which enhance the heat transfer [8, 31], but the rigidity of the AT may be affected increasing bending at high temperatures. The fins change the direction of the fluid flow to form a secondary flow based on the increased convection heat transfer area. A finned tube may slightly increase the cost of the overall power plant (~0.5%), but could improve the thermal efficiency by up to 2% [8, 28]. Therefore, adding fins in the inner wall of the AT is a highly potential way to strengthen heat transfer. Various types of fins have been proposed such as array pin fin [25], internal longitudinal fin [26, 27] and helical fin [28].

A lot of research has been done on the large-aperture PTC system which enhance heat transfer in the traditional circle AT, and thus has promoted the development of PTC. The literature review also demonstrates that the semi-circular AT with two external fins show the best and the highest efficiency for large-aperture PTCs [6]. However, one of the drawbacks of this design is much higher temperature (+50 ℃)at the edge of the fin than that in the HTF [6], which could damage the absorber on the edge of the fin and the damage will spread to the inner part, causing the coating failure on the surface of AT. Therefore, a modified design is introduced here in which the external fins are excluded and replaced by fins at the bottom of the semi-circular AT. This paper presents a comprehensive optical and thermal analysis of the new design, including a comparative study of fins with different geometries.

2 Heat transfer models

2.1 Geometric model of the absorber tube

The improved evacuated AT is composed of a semi-circular AT, a flat-plate radiation shield and a round glass cover (see Fig.1). The outer surface of the semi-circular part faces towards the aperture direction of the primary reflector (PR), the plane part faces away from the aperture direction of the condenser, and the center of the semi-circle is still at the focus of the PR [5, 6]. The flat-plate radiation shield is located in the vacuum part inside the glass cover and parallel to the AT's plane part, and its length (K) is larger than the diameter (2R) of semi-circular AT.

The semi-circle surface mainly intercepts the solar rays reflected by the PR. One of the most important purposes of the flat-plate radiation shield is to re-reflect the energy external radiation from the AT's flat surface back to the AT to reduce the external radiation loss, and another purpose is to reflect the rays that is not intercepted by AT's semi-circular surface onto the its flat part.
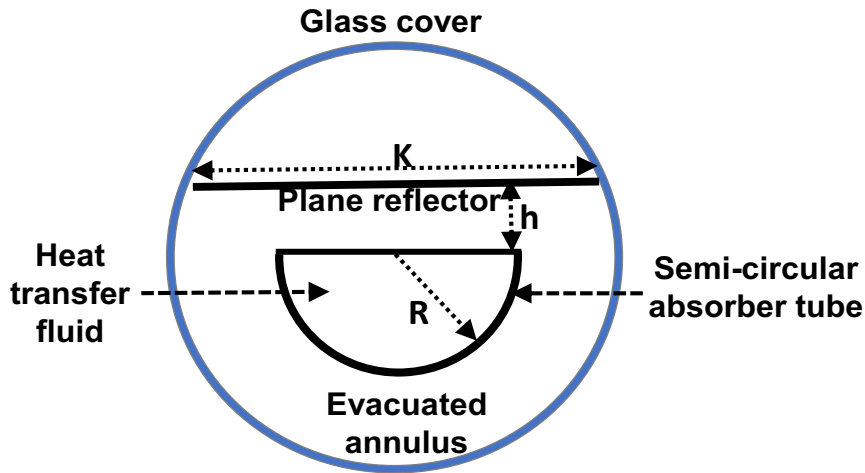

Figure 1. Cross-section of the semi-circular AT [6].

Where h is the distance form plat-plate radiation shield to plane part of AT.

2.2 Heat transfer enhancement model

The energy equation governing the convective heat transfer of the fluid inside the tube is as follows [41]:

$$\nabla(K_f \nabla T) = \rho c_p \frac{\partial T}{\partial t} + \rho c_p U \nabla T + \dot{\Phi} \tag{1}$$

Where T is the temperature; C_p is specific heat capacity at constant pressure; K_f is thermal

127 conductivity; ρ is density; $\dot{\Phi}$ is loss energy; t is time; U is velocity vector; and ∇T is temperature

128 gradient. The thermal energy introduced into the HTF through the AT's inner wall constitutes of three

129 terms: the energy from the temperature change of the HTF in the AT, the energy extracted by the HTF

130 and the energy losses.

131

132 Using a two-dimensional flow field as an example, where y is the direction of the temperature gradient

133 (heat transfer direction), the heat flux density (q) at the inner surface (y=0) can be obtained by

134 integrating Eq.(1) [41].

$$\text{q} = -K_f \frac{dT_f}{dy}\bigg|_{y=0} = \int \rho c_p (\frac{\partial T_f}{\partial t} + \text{u}\frac{\partial T_f}{\partial x} + \text{v}\frac{\partial T_f}{\partial y}) \; dy + \Phi \tag{2}$$

135

136

137 Where u and v are the velocity in x and y direction. As there is no fluid at the solid-liquid interface

138 (y=0), all heat introduced through the AT inner wall will be extracted by the HTF, so that Eq. (2) can

139 be simplified as follows [42, 43]:

$$\text{q} = -K_f \frac{dT_f}{dy}\bigg|_{y=0} = \int \rho c_p (\text{u}\frac{\partial T_f}{\partial x} + \text{v}\frac{\partial T_f}{\partial y}) \; dy \tag{3}$$

140

141

142 Multiplying Eq. (3) with the tube heat wall area (A) gives the total heat (Q) through the inner wall

143 [42, 43]. As the temperature gradient at the solid-liquid interface is in y-direction, the temperature

144 gradient in the x direction is 0 and $\frac{\partial T_f}{\partial x} = 0$. At the near wall surface (y=0), the thermal diffusion

145 coefficient $a = \frac{K_f}{\rho c_p}$ [42, 43]. Using the Prandtl number $p_r = \frac{\upsilon}{a}$, Q can be written in the following

146 form [42, 43]:

$$Q = -\text{A} \times K_f \frac{dT_f}{dy}\bigg|_{y=0} = A\frac{K_f \text{P}_r}{\upsilon} \int (|\vec{U}|\cos\beta\frac{\partial T_f}{\partial y}) \; dy \tag{4}$$

147

148

149 Where $\text{v} = |\vec{U}|\cos\beta$, β is the angle between fluid velocity ($\vec{U}$) and temperature gradient ($\frac{\partial T_f}{\partial y}$), and

150 υ is dynamic viscosity of HTF.

151

152 The amount of heat introduced into the AT is equal to that extracted by the HTF according to the Eqs.

(2)-(4), so increasing the amount of heat carried away by the fluid also increases the amount of heat introduced. Therefore, we can see from Eq. (4) heat transfer could be enhanced by the following means [42, 43]:

1. Increasing the temperature difference ($\frac{\partial T_f}{\partial y}$);

2. Increasing the fluid velocity ($\vec{U}$);

3. Increasing the heat transfer area (A);

4. Improving the physical properties of the heat transfer fluid, e.g. selecting a fluid with a high thermal conductivity (K_f);

5. Adjusting the angle (β) between the flow speed vector ($\vec{U}$) and the temperature gradient ($\frac{\partial T_f}{\partial y}$);

as close to zero as possible (cosβ=1) [42, 43].

Turbulent heat transfer dominates in the AT, and thermal resistance mainly exists in the laminar regime near the inner wall of AT accounting for about 70% of the total thermal resistance [41, 43]. So, heat transfer is dominated by heat conduction in the vicinity of the inner wall [43]. To enhance the heat transfer performance two fin configurations are studied here: "Long and thin " and "short and thick" as illustrated in Fig. 2. The two types of fins are named according to their shapes, the one with the larger ratio of length to diameter is named "long and thin" fin, and another with the smaller ratio is named "short and thick" fin.
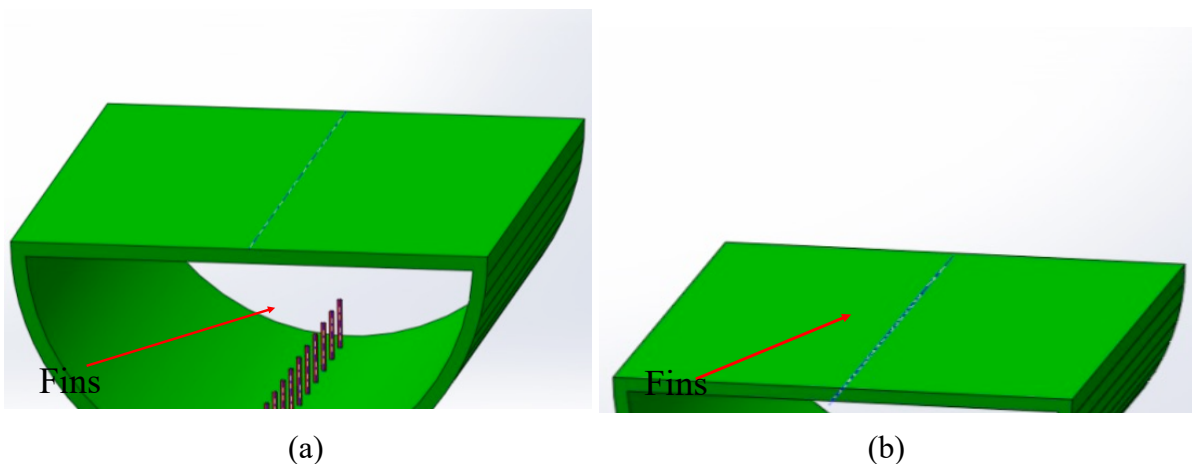

(a)   (b)

Figure 2. Diagram of two kind of fins to enhance heat transfer. (a) Long and thin fins, (b) short and thick fins.

2.3 Turbulence model for computational fluid dynamics

178

The Reynolds number is always above 3185 in our cases as the minimum fluid velocity is 0.5m/s meaning that the flow will be turbulent. The three-dimensional steady-state equations governing the flow include the continuity, energy, momentum, and k-ε equations [5, 6, 44, 45]:

Continuity equation：

$$\frac{\partial}{\partial x_i}\left(\rho u_i\right)=0 \tag{5}$$

Energy equation：

$$\frac{\partial}{\partial x_i}\left(\rho u_i T\right)=\frac{\partial}{\partial x_i}\left[\left(\frac{u}{Pr}+\frac{u_t}{\sigma_T}\right)\right]+s_h \tag{6}$$

Momentum equation：

$$\frac{\partial}{\partial x_i}\left(\rho u_i u_j\right)=\frac{\partial p}{\partial x_i}+\frac{\partial}{\partial x_i}\left[\left(u_t+u\right)\left(\frac{\partial u_i}{\partial x_j}+\frac{\partial u_j}{\partial x_i}\right)-\frac{2}{3}\left(u_t+u\right)\frac{\partial u_l}{\partial x_l}\delta_{ij}\right]+\rho g_i \tag{7}$$

k and ε equations:

$$\frac{\partial}{\partial x_i}\left(\rho u_i k\right)=\frac{\partial}{\partial x_i}\left[\left(u+\frac{u_t}{\sigma_k}\right)\frac{\partial k}{\partial x_i}\right]+G_k-\rho\varepsilon \tag{8}$$

$$\frac{\partial}{\partial x_i}\left(\rho u_i \varepsilon\right)=\frac{\partial}{\partial x_i}\left[\left(u+\frac{u_t}{\sigma_\varepsilon}\right)\frac{\partial\varepsilon}{\partial x_i}\right]+\frac{\varepsilon}{k}\left(c_1 G_k-c_2\rho\varepsilon\right) \tag{9}$$

$$u_t=c_u\rho\frac{k^2}{\varepsilon},\quad G_k=u_t\frac{\partial u_i}{\partial x_j}\left(\frac{\partial u_i}{\partial x_j}+\frac{\partial u_j}{\partial x_i}\right) \tag{10}$$

where σ_k, σ_ε = Prandtl numbers for the transport of turbulent dissipation rate ε/k; σ_T= Prandtl number for energy; c_1, c_2, c_u = constants in the k-ε turbulence model (c_1=1.44, c_2=1.92, c_u=0.99, σ_k=1.0, σ_ε=1.0 and σ_T=0.85); G_k = generation of turbulent kinetic energy; i, j, k = Cartesian coordinates and g =gravity acceleration [5, 6, 44, 45] .

Above equations are solved with the ANSYS 17.1 Computational Fluid Dynamics model (CFD) [5, 6, 8].

3. Optical analysis

The SolTrace-tool is used here to perform the optical simulations of the large-aperture trough. The tool has been developed by the National Renewable Energy Laboratory (NREL) in the United States for concentrating solar thermal power systems [46, 47]. It is widely used for CSP analysis [5, 6, 46, 47]. The parameters of the concentrator considered here are shown in Table 1. LS-3 solar tracking parameters were also used in SolTrace [5, 6]. To maximize the optical efficiency, the reflector parameters were adjusted to obtain a plate reflector length (K) of 130 mm and distance (h) of 21mm when the AT's radius (R) is 50 mm,

Table 1 Parameters for optical analysis [1, 5, 6].

Parameter	Value
Thickness of AT, H (mm)	3
Radius of the glass cover, D_{gla} (m)	0.0725
Trough aperture width, M (m)	8
Rim angle of trough, φ (°)	80
Focal length of trough, f (m)	2.3835
Absorptivity of the absorber coating, ξ_{abs}	0.96
Reflecting of the glass cover, ρ_r	0.97
Transmissivity of the glass cover, τ_{gla}	0.96
Specularity error of trough, σ_{spec} (mrad)	0.5
Direct normal irradiance (DNI), (W/m^2)	1000

3.1 Verification of the optical model

The tracking systems of LS-3 is adopted here [5, 6]. The optical efficiencies obtained from the numerical simulation are 83.3%, 74.7% and 80%, respectively, which are consistent results from [5-7] indicating that the method of modeling approach with SolTrace-tool used in this paper is satisfactory. Secondly, the optical model in this paper is optimized on the basis of [6] and removing two external fins (see Fig. 1). The maximum solar radiation flux obtained here and in [6] are found at the lowest end of the semicircle, and these maximum values are 46419W/m^2 and 46356 W/m^2, with just a 0.14% difference. The outcome of the optical simulation in this paper is thus very close to those in [6].

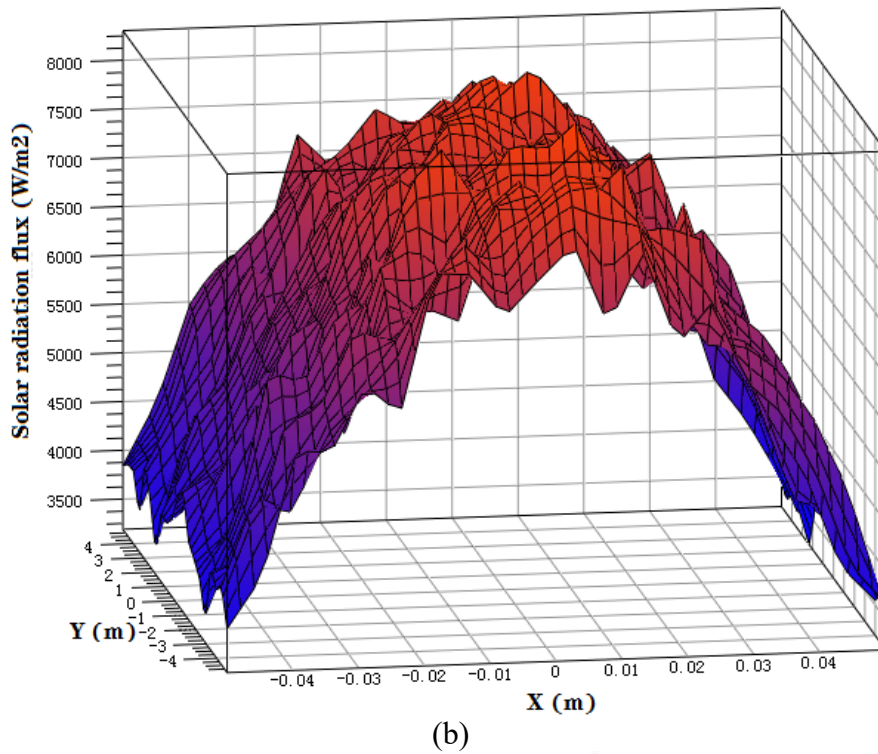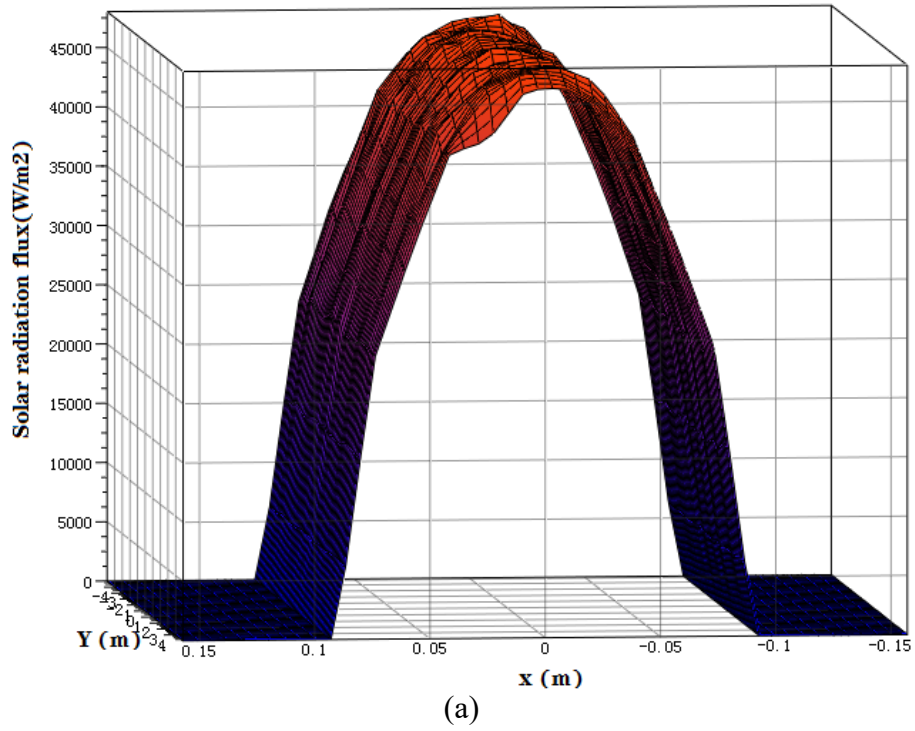## 3.2 Optical analysis of the AT surface

(a)

(b)

Figure 3. Solar radiation flux on surface of the AT. (a) Semi-circle part, (b) Plane part.

Figure 3 shows the solar radiation flux on the absorber tube. The average solar radiation flux (E_{ave}) on the semi-circular and plane part of the AT are 36558 W/m^2 and 5912 W/m^2, respectively. The optical efficiency (η_{opt}) of the large-aperture trough solar concentrator system can be calculated from the following relation [5, 6, 8]:

$$\eta_{\mathrm{opt}} = \frac{E_{ave1} \times \pi \times R + E_{ave2} \times 2R}{NDI \times M} \tag{11}$$

Where E_{ave1} and E_{ave2} are the average solar radiation flux on the semi-circle and plane part of the AT, respectively. Using Eq. (11), an optical efficiency of 79.2% was obtained, with 71.8% from the semi-circle part and 7.4% from the flat part. Thus, the semi-circular part contributes almost ten times more than the flat part to the total solar flux on the AT. Actually, the energy balance of the plane part is negative energy as the energy radiated outside from it is greater than the solar energy absorbed. Therefore, adding a flat-plate radiation shield in this area can reduce the radiation losses and improve the thermal efficiency of the concentrator [6].

The solar radiation flux on the surface of the semi-circular and the flat part of the AT is symmetrically distributed (see Fig. 3). The maximum flux (46356W/m^2, see Fig. 3a) is found on the bottom of AT, while the minimum value (4000 W/m^2, Fig.3b) is found at the two edges of the flat part. As the ratio of the maximum to the minimum value of the energy flux on the AT's surface is about ten, will mean that the energy flow density is not uniform. The heat flux on the plate surface is rough compared to the semi-circular surface (see Fig. 3), which also indicates that the semi-circle part mainly absorbs the sun rays and the flat part is just an auxiliary function.

4. Thermal analysis

For the thermal analysis of the AT, the following set of boundary conditions and assumptions are employed:

(1) The circumferential heat flux on the AT surface is given by Fig. 3, and the AT's length (L) is 0.120m with a roughness of 0.15mm;

(2) The x-direction velocity of the flow is 0.05-1.5 m/s and in other directions is 0 [5, 6];

(3) A mixture of salt (60%NaNO$_3$+40%KNO$_3$) is used for the HTF with temperature range 300℃-600℃ and the thermo physical parameters shown in formula (12) is adopted in this paper [5, 6].

$$\begin{cases} \rho = 2090\text{-}0.636T \\ C_p = 1443 + 0.172T \\ K_f = 0.443 + 1.9 \times 10^{-4}T \\ v = 22.714 \times 10^{-3} - 0.12 \times 10^{-3}T + 2.281 \times 10^{-7}T^2 - 1.474 \times 10^{-10}T^3 \end{cases} \tag{12}$$
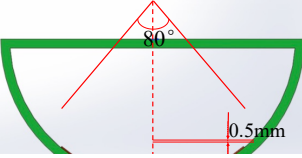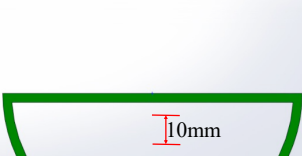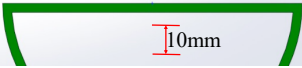
269   Where v=dynamic viscosity 10^{-3}N S/m^2.

270 (4) A mixed boundary of convection and radiation is employed on the absorber tube [5, 6]. The

271   convective heat transfer coefficient between the AT surface and the atmosphere is 0.112 mW/m^{2}K

272   [5, 6]. The ambient temperature is set to 300K, the sky temperature is 287K. The emissivity (ε_{abs})

273   of the surface of the AT semi-circle is 0.094 at 673.15K [1, 5, 6], and the emissivity (ε_{abs}) of the

274   plane part is 0.00282 [5, 6];

275 (5) Other geometric and optical parameters are shown in Tables 1 and 2.

277 <div align="center">Table 2. Geometrical parameters of the fins.</div>

Figure	Type of fin	Fin diameter (mm)	Fin height (mm)	Fin spacing[1] (mm)	Fill rate[2] 10^{-4} (-)	Expansion[3] 10^{-4} (1/mm)
	No fin	0	0	0	0	0
	Short and thick fins	1	0.5	10	13.46	53.86
	Long and thin fins (I)	1	10	10	4.10	16.41
	Long and thin fins (II)	1	10	20	2.05	8.21

279 [1]Fin spacing: the distance between two adjacent fins

280 [2] Fill rate: the volume of fins per unit volume of heat transfer space of (-)

281 [3] Expansion: the surface area of fins per unit volume of heat transfer space (1/mm)

4.1 Validation of the thermal model

285 The thermal models were incorporated into a commercial computational fluid dynamics software

286 ANSYS Fluent 17.1 [5, 6, 48, 49]. The meshing tool of ANSYS 17.1 was used to generate structured

287 hexahedral and unstructured tetrahedral meshes shown in Fig. 4. The structured hexahedral grid

288 dominate the mesh and the unstructured grid is mainly used near the fins [48, 49]. The pressure-based

289 solver in Fluent was employed to solve Eqs. (5)-(10) with the boundary described previously [5, 6].

290 The SIMPLE algorithm was used for solving the coupled pressure and velocity [48, 49]. The

291   governing equations were integrated using the second order upwind scheme.

292

293   Thermal efficiency and resistance are the two main evaluation indicators in this paper, and changes

294   with the number of grids are shown in Table 3. The changes in thermal efficiency and pressure drop

295   from inlet and outlet are very small which can be ignored, indicating that it can fully satisfy the

296   simulation demand using the mesh in Table 3. Therefore, this paper chooses the one with the larger

297   number of grids in Table 3 in different cases to meet simulation demand.

298
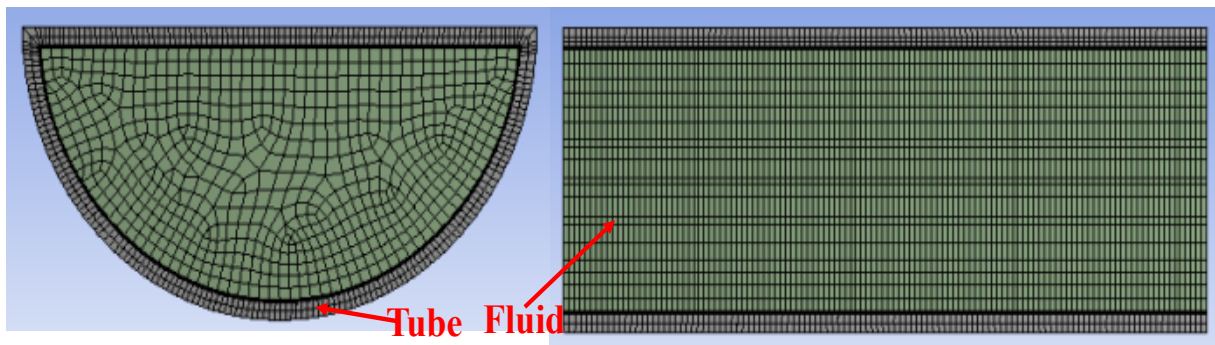
(a)
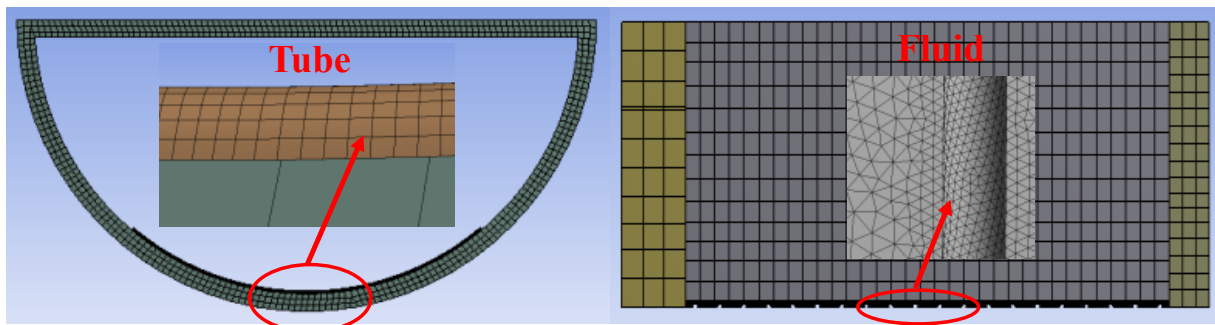
(b)
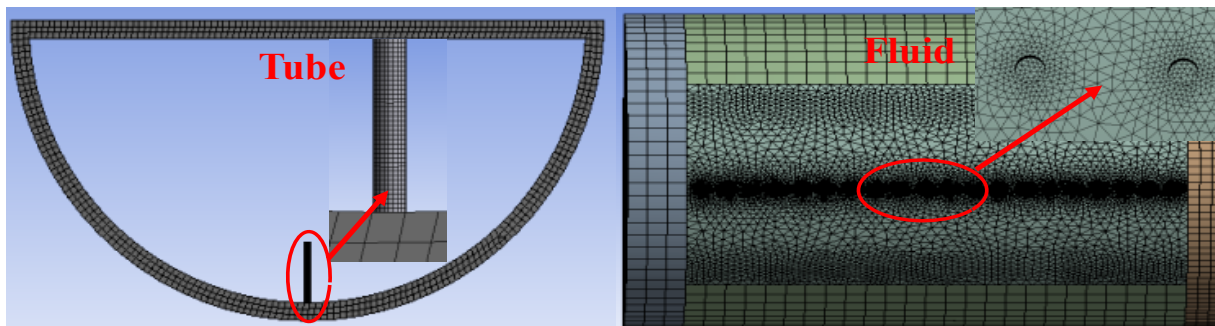
(c)

Figure 4. Illustration of the structured and unstructured mesh for the CFD analysis. (a) No fin. (b) Short and thick fins. (c) Long and thin fins.

Table 3. Grid independence verification

	Mesh number	Thermal efficiency (%)	Pressure difference between inlet and outlet (Pa)
Finless AT	225870	75.7	63.7
	211470	75.8	63.6
Finned AT	5339959	76.9	93.2
	5332775	77.1	94.1

310

311 **Validation of the AT model without fins**

312

313 The finless AT model is optimized on the basis of [6] removing the two external fins to protect the

314 coating on the AT's surface from overheating. The optical efficiency is reduced from 83.3% [6] to

315 79.2% (see Table 4). The thermal efficiency of 75.7% given in this paper for the case without outer

316 fins is less than 80.3% with the two fins [6] (see Table 4) indicating that the numerical simulation

317 done here is sensible. The AT is a semi-circular of 50mm radius both here and in [6], so the energy

318 loss when moving from the optical to thermal efficiency is quite similar. This loss is here 3.5 %

319 whereas [6] gives 3%, i.e. quite close which supports the validity of the numerical simulation.

320

321 The circumference of the AT in this article consists of a 157.1 mm semi-circle part and 100mm pane

322 part which together is close to the 219.9mm of the 70 mm AT. Therefore, the external radiation losses

323 are quite similar the difference being 1.1% (4.6%-3.5%=1.1%) (see Table 4), which further shows

324 confirms the validity of the simulation.

325

326 Table 4. Parameters for model validation of smooth AT.

	Inlet temperature T_{in} (K)	AT's length L (m)	Circumferential length (mm)	Coating emissivity ε_{abs}	Optical Efficiency η_{opt} (%)	Thermal efficiency η_{th} (%)	Efficiency loss η_{lost} (%)
This model	673.15	0.12	157.1+100[*]	0.094+0.00282	79.2	75.7	3.5
Ref. 6	673.15	4	177.1+120	0.094+0.00282	83.3	80.3	3
Ref. 5	673.15	4	219.9	0.094	74.7	70.1	4.6

327 [*] The semi-circular AT is divided into a semi-circular part and a flat part

328

329 **Validation of the AT model with fins**

330

331 Bellos et al. proposed that the thermal efficiency can been improved 0.5%-2% by enhancing heat

332 transfer using e.g. fins [8]. The thermal efficiency increased by 1.23% and 1.6% after adding two

333 different types of fins in this article, which fits the previous observations. Bellos et al [8, 26, 39]

found that thin and long fins can increase the thermal efficiency by 1.5% using Syltherm 800 as HTF. The thermal efficiency was increased by 1.6% in this paper when using long and thin fins, indicating that the numerical calculation of long thin fins model is sound. Bellos et al. [8, 26, 39] showed an improvement of 0.69% in the thermal efficiency, which is close to that obtained by present model, or 0.75% (see Table 5) under similar geometric dimensions and boundary conditions. In case of short and thick fins with 5mm height and 6mm diameter, the improved thermal efficiency was 0.43% [8,26,39], which is also close to the 0.39% in this article, though here the dimensions were smaller. These comparisons confirm the consistency of the numerical model with previous studies.

Table 5. Model validation of ATs with different fins.

Categories	Model	Inlet temperature T_{in} (K)	Fin size for diameter/height (mm)	Fluid velocity	Increased thermal efficiency (%)
Long and thin fins	This model	673.15	1/10	0.7 m/s	0.75
	Bellos [8,26,39]	600	2/20	150 l/min	0.69
Short and thick fins	This model	673.15	1/0.5	0.7 m/s	0.39
	Bellos [8,26,39]	600	6/5	150 l/min	0.43

4.2 Thermal analysis of AT with two fins

Figure 5 shows the surface temperature of the absorber tubes for different fins geometries, clearly indicating that the temperature decreases with increasing flow rate (the Reynolds number increases), also providing protection to the surface coating [5, 6]. However, the pressure drops (∇P) in the AT increases simultaneously, thus increasing the pumping power [6].
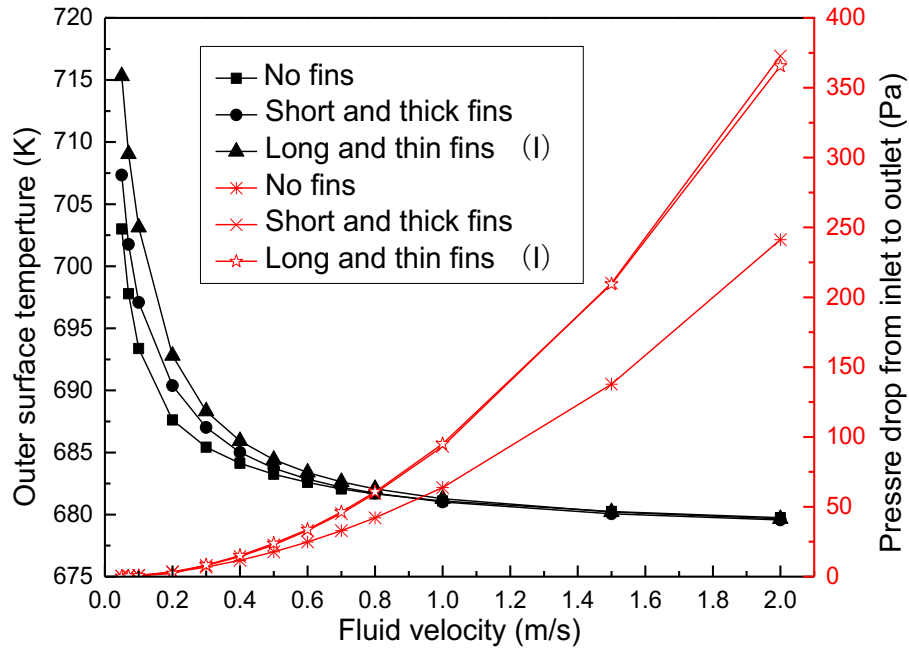
Figure 5. Changes of surface temperature and pressure drop from inlet to outlet as function of flow rate.

Above a fluid velocity of 0.5m/s (Re=31855), the temperature decreases slowly, but the pressure drop increases quickly as shown in Fig. 5. For example, when the fluid speed rises from 0.05m/s (Re =3185) to 2m/s (Re=127420), the AT's surface temperature drops by 23.3℃ (no fins), 27.8℃ (short and think fin) and 35.6 ℃(long and thin fin I), respectively, and the pressure increases by 240.9 Pa (no fins), 372.5 Pa (short and think fin) and 365.4 Pa (long and thin fin I). However, when the fluid speed is increased from 0.5m/s (Re=31855) to 2m/s (Re=127420), the surface temperature decreased only by 3.5℃ (no fins), 4.2℃ (short and think fin), and 4.8℃ (long and thin fin I) respectively, but the pressure drop grew by 223.6 Pa (no fins), 349.9 Pa (short and think fin) and 341.8 Pa (long and thin fin I). This shows that it is very difficult to reduce the AT's surface temperature by increasing the flow velocity above 0.5m/s. To avoid any damage in the AT, the minimum flow rate should be set in this case at 0.5m/s (DNI=1000 W/m^2). To keep the outlet temperature the same under varying solar intensity, the flow rate should be adjusted accordingly.

The thermal efficiency (η_{th}) was determined using Eq. (13) [8]:

$$\eta_{th} = \frac{Q_u}{DNI \times M \times L} \tag{13}$$

The solar heat output (Q_u) output was obtained from the ANSYS Fluent 17.1 simulation and L is the length of AT.
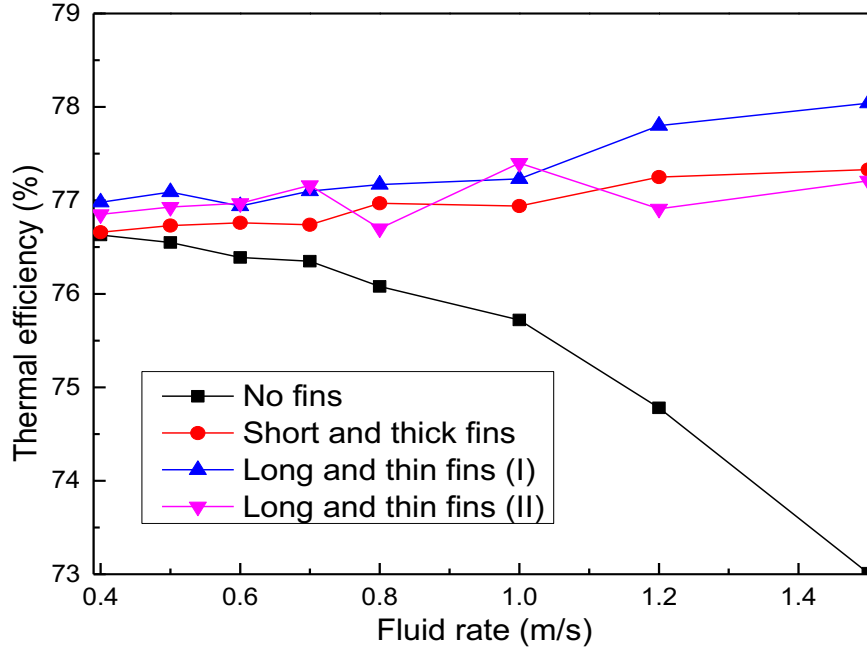
374

Figure 6. Variation of the thermal efficiency with flow rate.

376

Figure 6 shows the thermal efficiency for the range of relevant flow rate values. The average thermal efficiency is 75.7% (no fins), 76.9% (short and thick fin) and 77.3% (long and thin fin I). The thermal efficiency has increased by 1.2% (short and thick fin) and 1.6% (long and thin fin I) compared to the no fins case. The pressure drop increased by adding fins to AT (see Fig. 5), but the difference between the two kinds of fins was negligible. The long and thin fined AT have higher friction losses, because most of the fins penetrate into the area where the fluid velocity is high thus causing a higher frictional loss is large. Whereas, the short and thick fins are close to the inner wall surface of the AT and most of them are in the viscous bottom layer, where the flow velocity is low and close to 0 at the solid-liquid interface, leading to low frictional loss. The long and thin fins show better heat transfer enhancement and a higher thermal efficiency in the flow range 0.4-1.5m/s.

387

Figure 6 shows that the thermal efficiency is improved after adding fins to the absorber tube mainly because of the combined effect of the temperature gradient ($\frac{\partial T}{\partial y}$), convective heat transfer area (A) and the angle (β) between the speed vector ($\vec{U}$) and the temperature gradient in Section 2.2 for the heat transfer enhancement [42, 43]. The increase of the heat transfer area of the AT with short and long fins is about three times that of thin and long fins (see Table 2), but the AT with thin and long fins have a higher heat transfer efficiency than with short and thick fins, explained by the temperature difference driving force and the effect of field synergies (cosβ). The temperature difference of the

convection heat transfer of thin and long finned (I) tubes is 0.38K higher than with short and thick finned tubes (see Fig.7), and the thermal efficiency is improved by 0.37%.
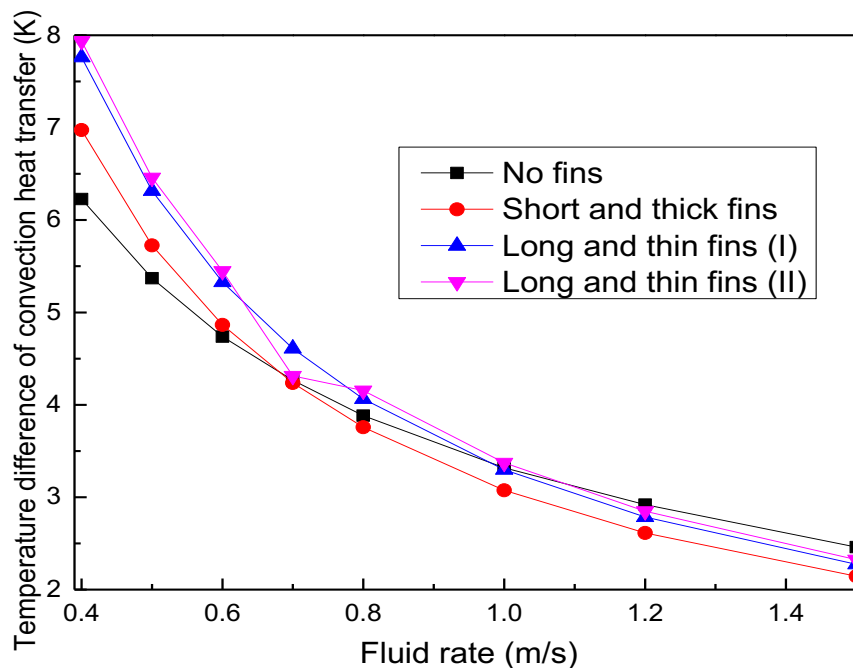
The direction of the velocity and temperature around the fins are changed when adding fins to the AT (Fig.8). According to the field synergy theory [42, 43], heat transfer performance is enhanced if the angle (β) between the velocity and temperature gradient is close to 0° [42, 43]. Fig. 8(a) shows that for short and thick fins a part of the velocity is in opposite direction to the flow field at the solid-liquid interface so that β >90° (cosβ<0), which weakens the heat transfer enhancement. Fig. 8(b) for long and thin fins shows that a small part of the fluid velocity points to the inside of the fin thus weakening the heat transfer. However, as β<90° heat transfer will be enhanced. As shown in Fig. 6, the long and thin finned tube has higher heat transfer enhancement and thermal efficiency, because the angle β is close to 0 (Fig.8b) and the velocity of the fluid on the surface of the long and thin fins is vertical or close to vertical to the convective heat transfer surface in Fig.8 (b). Therefore, based on the above, the field synergy (the angle between the velocity direction and the temperature direction) plays a key role for the heat transfer enhancement.
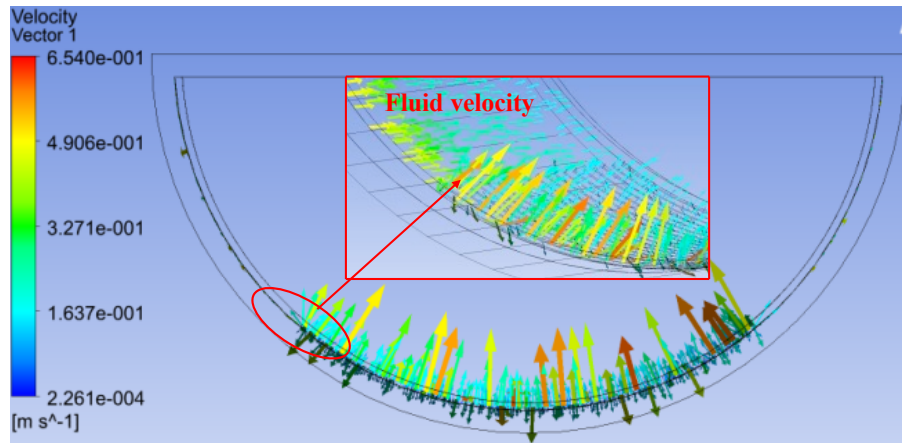
The thermal efficiency of the no fins case decreases when increasing the flow velocity (Fig. 6), because the temperature difference of the convective heat transfer decreases (Fig. 7). However, a lower AT surface temperature would protect the AT surface coating from overheating with a larger fluid rate.

(a)

(b)
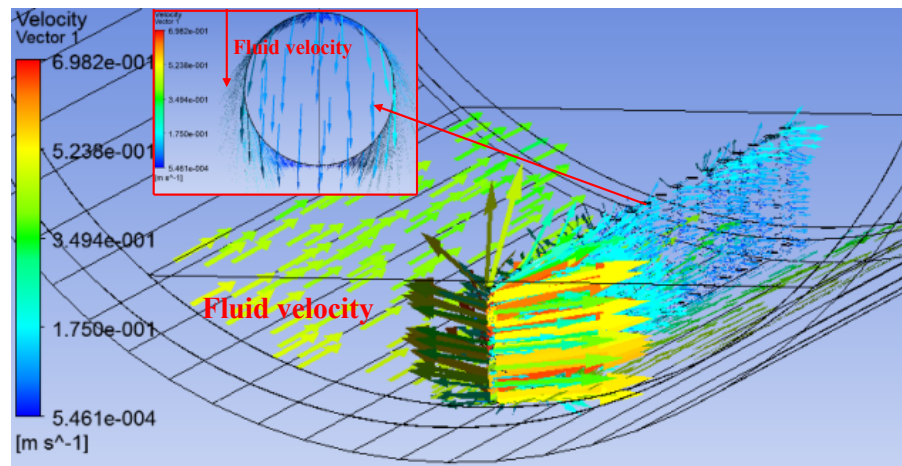
Figure 8. The direction of fluid flow at the surface of convective heat transfer for fluid velocity of 0.5m/s. (a) Short and thick fins. (b) Long and thin fins.

4.3 Analysis of heat transfer enhancement

As shown in previous Section, the thermal efficiency of the AT is improved when adding fins, but with a penalty that the pressure drop increases (see Figs. 6, 9-10). The ratio of the thermal efficiency of the fin to no fins is shown in Fig. 9, indicating a thermal efficiency improvement if the ratio is >1. The maximum value is close to 1.07 contributed by the long and thin fins (I) at a speed of 1.5 m/s. The ratio of the pressure drops (Fig. 10) is always > 1.1, reaching 1.5 at 1.5 m/s. Therefore, a more comprehensive analysis of the heat transfer enhancement is justified.
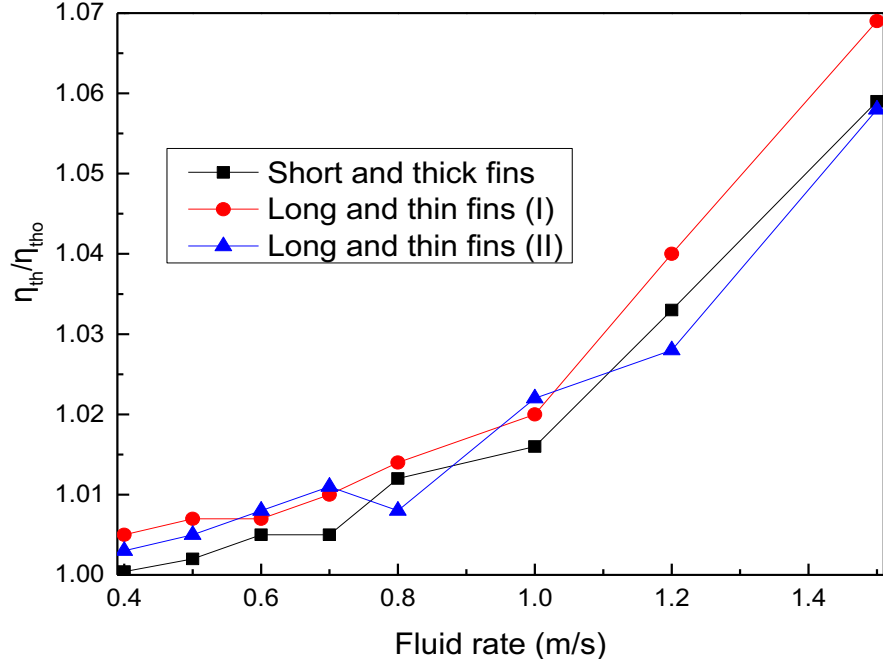
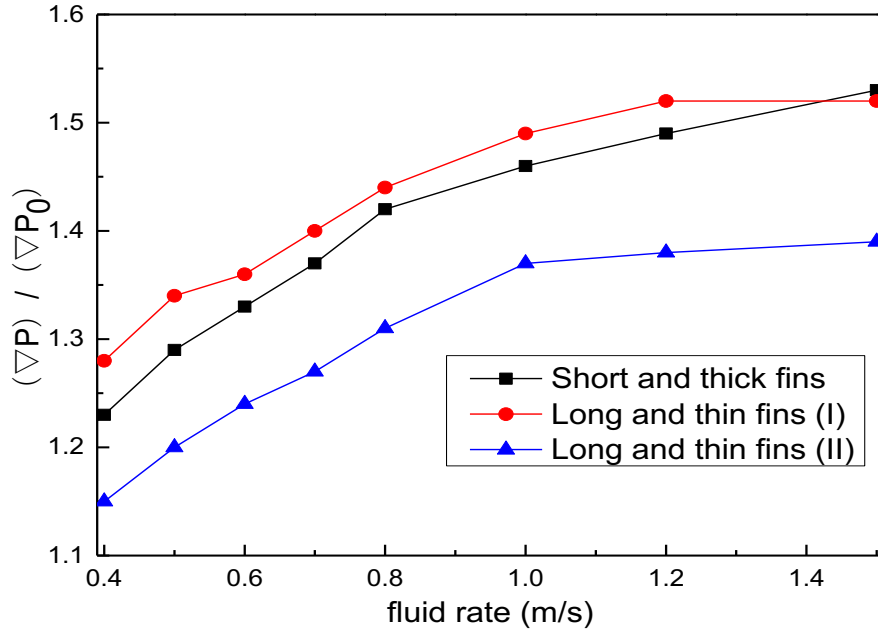Figure 9. Ratio of the thermal efficiency of the finned AT to smooth AT.

Figure 10. Ratio of the pressure drop of the finned AT to smooth AT.

To estimate the heat transfer improvement through the fins, a heat transfer performance factor (η_{HTP}) is defined as follows [6, 26, 27]:

$$\eta_{\text{HTP}} = \frac{(Nu/Nu_0)}{(f/f_0)^{\frac{1}{3}}} \tag{14}$$

444 Where h_f is the heat transfer coefficient and Nu is Nusselt number. $\eta_{HTP} > 1$ indicates that the overall

445 performance is improved by adding fins; $\eta_{HTP} < 1$ means that increasing pumping power requirement

446 exceeds the thermal enhancement [6, 25].

447

448 The individual terms in Eq.(14) are calculated through the following equations:

449 The heat transfer coefficient (h_f) between the HTF and the inner surface of AT is defined as [25, 26]:

450
$$h_f = \frac{Q_u}{\pi \times D_{ri} \times L \times (T_r - T_{fm})} \tag{15}$$

451

452 where the average temperature (T_{fm}) of the HTF in the AT is the following [26, 27]:

453
$$T_{fm} = \frac{T_{out} - T_{in}}{2} \tag{16}$$

454 The Nusselt number (Nu) is defined as [26, 27]:

455
$$Nu = \frac{h_f \times D_{ri}}{k} \tag{17}$$

456 The friction factor (f) is calculated as [26, 27]:

457
$$f = \frac{\Delta p}{\frac{1}{2}\rho \times U^2} \times (\frac{D_{ri}}{L}) \tag{18}$$

458 Where D_{ri} is the inner diameter of AT, T_{in} is the inlet temperature, T_{out} is the outlet temperature, and

459 ρ is the fluid density at average temperature.

460 The simulation results from Fluent 17.1 are substituted into Eqs. (15)-(18), yielding then the heat

461 transfer performance factor (η_{HTP}) which is shown in Fig. 11. The heat transfer performance factor

462 (η_{HTP}) exceeds 1 at a flow velocity of 1.2m/s for short and thick finned AT and at 1.5 m/s for long

463 and thin finned AT. The main factors for $\eta_{HTP} < 1$ at low flow rates can be attributed to the pressure

464 drop between the inlet and outlet (friction factor) and the larger temperature difference of convection

465 heat transfer with fins (see Fig.7). The heat transfer performance factor (η_{HTP}) of short and thick

466 finned AT is always higher than that of the long and thin finned AT due to a lower temperature

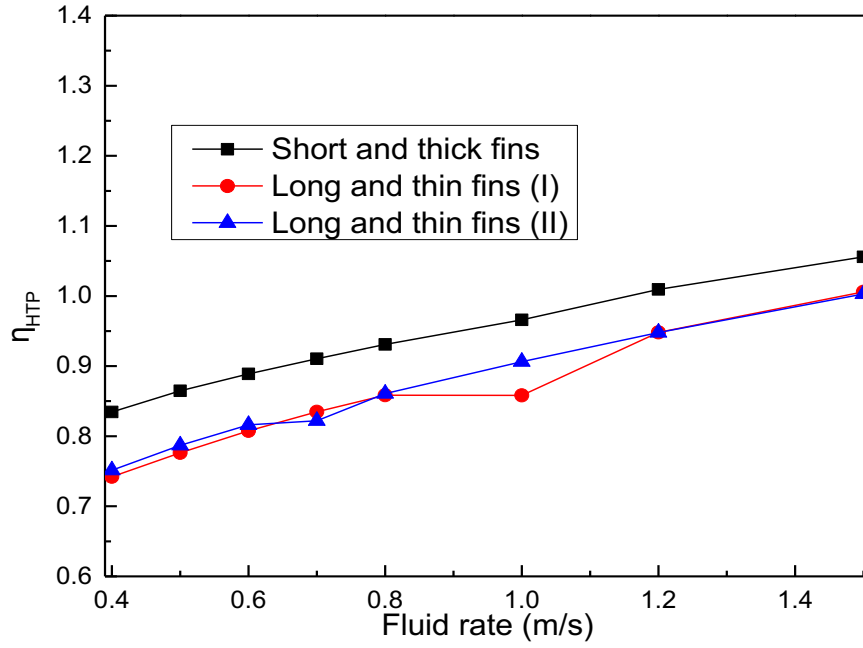467 difference in convective heat transfer.

Figure 11. Heat transfer performance factor for using fins.

4.4 Analysis of heat transfer performance of long and thin fins

As shown earlier in Table 2, increasing the fin spacing of long and thin finned AT reduces the thermal efficiency (see Figs. 6 and 9). For example, when the fin spacing is increased from 10mm to 20mm, the number of fins is reduced from 20 to 10, and the thermal efficiency is reduced from 77.29% to 77.02% (see Fig.6) but the pumping power consumption (pressure drop) is also increased. By doubling the number of fins (see Table 2), the thermal efficiency increased by 0.27% only (Fig.6), and the differences in of convective temperature difference is very small (0.05K) over the whole fluid velocity range (Fig.7). Thus, the heat transfer performance factor (η_{HTP}) for the long and thin finned AT with different spacing is almost identical (Fig.11), meaning that increasing the number of fins only marginally improves the heat transfer performance.

In Fig.12, we show the velocity profile around the long and thin fins. The fluid bypasses the fin surface from point A to point B, and a new fluid velocity is formed around the fins at the inlet, in the middle, and at the outlet as shown in Fig. 12. Heat is transferred to the fluid through the fin surface, so the direction of the temperature gradient is perpendicular to the fin surface. From the inlet to the outlet, the fluid velocity on the fin surface gradually becomes smaller (Figs. 8(b) and 12), mainly because the fluid needs to overcome the friction force when passing through the fin surface.

Point B in Fig.12 shows that the direction of the fluid velocity changes from pointing to inside of the

23

fin to pointing to the outside of the fin when moving from the inlet to the outlet, and the angle (β) between the directions of the flow velocity and temperature gradient is from 180° to 0°. According to the field synergy theory in Section 2.2, the more heat is transferred at point B during the process from inlet to the outlet, the stronger is the enhancement of heat transfer [42, 43]. The fluid velocity at point A is directed to the inside of the fin, hampering heat transfer at point A. However, the speed at point A decreases from the inlet to the outlet, and this obstruction will therefore gradually decrease. Both points A and B show that the convective heat transfer gradually increases from the inlet to the outlet, i.e., the enhancement of heat transfer gradually increases.
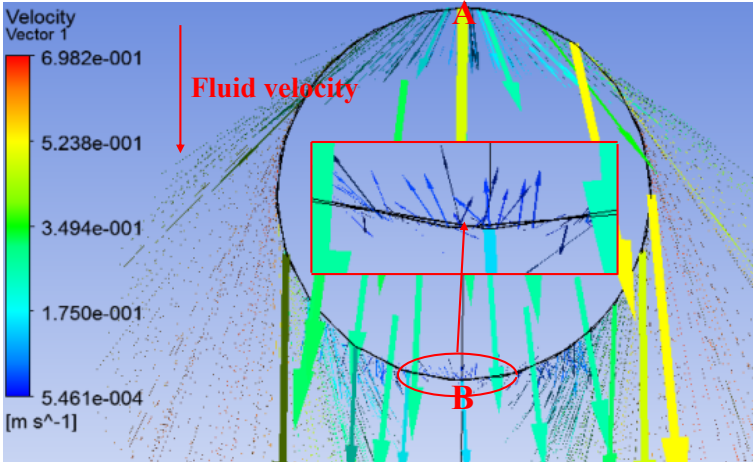
(a)
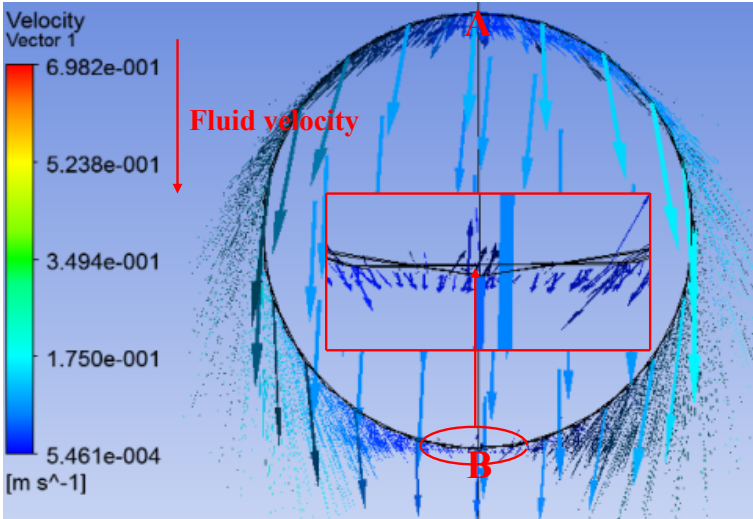
(b)
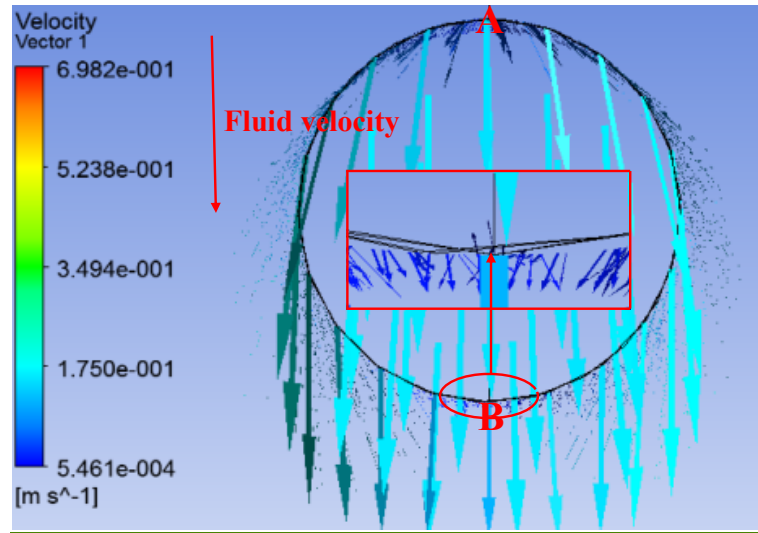
(c)

Figure 12. Velocity diagram around the long and thin fins. Fins are located (a) at the inlet, (b) in the middle, and (c) at the outlet.

5. Conclusions

A new design of an evacuated absorber tube consisting of a semi-circular with a radius of 50mm is proposed for an 8m width large-aperture parabolic trough concentrator. A flat-plate radiation shield 130mm wide is located in the vacuum part in the glass cover parallel to the plane part of the AT with a distance of 21mm. Two types of fins were added to the bottom of the AT to enhance heat transfer: Short and thick fins and long and thin fins. The optical, thermal and heat transfer performance of the fins were analyzed with the following conclusions:

- An absorber tube with no fins had an optical efficiency of 79.2% and a thermal efficiency of 75.7%. To avoid excessively high temperature in the AT, the fluid velocity should exceed 0.5m/s, while the friction factor is also small in AT;
- The thermal efficiency was has increased by 1.23% with short and thick finned AT and 1.6% with long and thin finned AT compared to an AT without fins. The long and thin finned AT showed a higher heat transfer enhancement but with much higher frictional losses than the short and thick finned AT;
- The heat transfer performance factor (defined as the ratio of heat transfer enhancement to change in frictional losses) of short and thick fins was higher than that of the long and thin fins, because of the lower frictional losses. The η_{HTP} exceeds 1 at a fluid rate of 1.2m/s for short and thick fins, and at 1.5 m/s for long and thin finned AT;

25

- Increasing the number of fins in a long and thin finned AT would only marginally enhance the heat transfer performance.

There are no exception some deficiencies which need to be further improved in this article. The semi-circular AT increases the thermal efficiency and avoids the appearance of high temperature. However, the AT's cross-sectional moment of inertia decreases when changing from a circular to a semi-circular, so it tends to bend at high temperature due to a larger linear expansion coefficient of the material. Therefore, it is necessary to continue to reduce the degree of bending. At the same time, although long and thin fins have higher efficiency, they extend further into the liquid, which leads to poor stability due to a larger ratio of length to diameter. Moreover, these fins are easy to bend by the fluid at relatively high flow rates, while they stay more stable when flow rate is low. Conversely, short and thick fins are more suitable for high flow rate occasions due to the good stability, but they have a relatively poor heat transfer enhancement effect.

Acknowledgement

References

[1] Mwesigye A, Meyer JP. Optimal thermal and thermodynamic performance of a solar parabolic trough receiver with different nanofluids and at different concentration ratios. Applied Energy 193 (2017) 393–413.

[2] Wang CL, Gong JH, Yan JJ, Zhou Y, Fan DW. Theoretical and experimental study on the uniformity of reflective high concentration photovoltaic system with light funnel. Renewable Energy 133 (2019) 893–900.

[3] Gong JH, Wang CL, Gong CY. Study on the uniformity of high concentration photovoltaic system with array algorithm. Solar Energy 153 (2017) 181-187.

[4] He YL, Wang K, Qiu Y, Du BC, Liang Q, Du S. Review of the solar flux distribution in concentrated solar power: Nonuniform features, challenges, and solutions. Applied Thermal Engineering 149 (2019) 448-474.

[5] Gong JH, Wang J, Lund PD, Hu EY, Xu ZC, Liu GP, Li GS. Improving the performance of a 2-stage large aperture parabolic trough solar concentrator using a secondary reflector designed by adaptive method. Renewable Energy 152 (2020) 23-33.

[6] Gong JH, Wang J, Lund PD, Zhao DD, Hu EY, Jin W, Improving the performance of large-aperture parabolic trough solar concentrator using semi-circular absorber tube with external fin

and flat-plate radiation shield. Renewable Energy 159 (2020) 1215-1223.

[7] Manikandan GK, Iniyan S, Ranko G. Enhancing the optical and thermal efficiency of a parabolic trough collector– A review. Applied Energy 235 (2019) 1524–1540.

[8] Bellos E, Tzivanidis C. Alternative designs of parabolic trough solar collectors. Progress in Energy and Combustion Science 71 (2019) 81–117.

[9] SkyTrough product information: next-generation solar parabolic tough technology. www.skyfuel.com/downloads/brochure/SkyTroughBrochure.pdf.

[10] Hoste G, Schuknecht N. Thermal efficiency analysis of Sky Fuel's advanced, large-aperture, parabolic trough collector. Energy Procedia 69 (2015) 96–105.

[11] Bennett W, Lun J, Jonathan F, Roland W. Experimental performance of a two-stage (50X) parabolic trough collector tested to 650 °C using a suspended particulate (alumina) HTF. Applied Energy 222 (2018) 228–243.

[12] Bennett W, Lun J, Jonathan F. Theoretical and experimental performance of a two-stage (50X) hybrid spectrum splitting solar collector tested to 600 °C. Applied Energy 239 (2019) 514–525.

[13] David RS, Gary R. Improving the concentration ratio of parabolic troughs using a second-stage flat mirror. Applied Energy 159 (2015) 620–632.

[14] Diogo C, Julio C, Manuel CP. New second-stage concentrators (XX SMS) for parabolic primaries; Comparison with conventional parabolic trough concentrators. Solar Energy 92 (2013) 98–105.

[15] Canavarroa D, Chavesb J, Collares-Pereiraa M. New optical designs for large parabolic troughs. Energy Procedia 49 (2014) 1279–1287.

[16] Mwesigye A, Bello-Ochende T, Meyer JP. Heat transfer and entropy generation in a parabolic trough receiver with wall-detached twisted tape inserts. International Journal of Thermal Sciences 99 (2016) 238–57.

[17] Zhu X, Zhu L, Zhao J. Wavy-tape insert designed for managing highly concentrated solar energy on absorber tube of parabolic trough receiver. Energy 141 (2017)1146–55.

[18] Sahin HM, Baysal E, Rıza Dal A, Sahin N. Investigation of heat transfer enhancement in a new type heat exchanger using solar parabolic trough systems. International Journal of Hydrogen Energy 40 (2015) 15254–15266.

[19] Song X, Dong G, Gao F, Diao X, Zheng L, Zhou F. A numerical study of parabolic trough receiver with nonuniform heat flux and helical screw-tape inserts. Energy 77 (2014) 771–782.

[20] Bellos E, Tzivanidis C. Investigation of a star flow insert in a parabolic trough solar collector. Applied Energy 224 (2018) 86–102.

[21] Jamal-Abad MT, Saedodin S, Aminy M. Experimental investigation on a solar parabolic trough collector for absorber tube filled with porous media. Renewable Energy 107 (2017) 156–163.

[22] Mwesigye A, Bello-Ochende T, Meyer JP. Heat transfer and thermodynamic performance of a parabolic trough receiver with centrally placed perforated plate inserts. Applied Energy 136 (2014) 989–1003.

[23] Nems´ M, Kasperski J. Experimental investigation of concentrated solar air-heater with internal multiple-fin array. Renewable Energy 97 (2016) 722–730.

[24] Cheng ZD, He YL, Cui FQ. Numerical study of heat transfer enhancement by unilateral longitudinal vortex generators inside parabolic trough solar receivers. International Journal of Heat and Mass Transfer 55 (2012) 5631–5641.

[25] Gong XT, Wang FQ, Wang HY, Tan JY , Lai QZ, Han HZ. Heat transfer enhancement analysis of tube receiver for parabolic trough solar collector with pin fin arrays inserting. Solar Energy 144 (2017) 185–202.

[26] Bellos E, Tzivanidis C, Tsimpoukis D. Thermal enhancement of parabolic trough collector with internally finned absorbers. Solar Energy 157 (2017) 514–31.

[27] Bellos E, Tzivanidis C, Tsimpoukis D. Optimum number of internal fins in parabolic trough collectors. Applied Thermal Engineering 137 (2018) 669–677.

[28] Munoz J, Abánades A. Analysis of internal helically finned tubes for parabolic trough design by CFD tools. Applied Energy 88 (2011) 4139–4149.

[29] Wang FQ, Tang ZX, Gong XT, Tan JY, Han HZ, Li BX. Heat transfer performance enhancement and thermal strain restrain of tube receiver for parabolic trough solar collector by using asymmetric outward convex corrugated tube. Energy114 (2016)275–292.

[30] Wang FQ, Lai QZ, Han HZ, Tan JY. Parabolic trough receiver with corrugated tube for improving heat transfer and thermal deformation characteristics. Applied Energy 164 (2016) 411–424.

[31] Huang Z, Li ZY, Yu GL, Tao WQ. Numerical investigations on fully-developed mixed turbulent convection in dimpled parabolic trough receiver tubes. Applied Thermal Engineering 114 (2017) 1287–1299.

[32] Bellos E, Tzivanidis C, Antonopoulos KA, Gkinis G. Thermal enhancement of solar parabolic trough collectors by using nanofluids and converging-diverging absorber tube. Renewable Energy 94 (2016) 213–222.

[33] Loni R, Askari Asli-ardeh E, Ghobadian B, Kasaeian AB, Gorjian Sh. Thermodynamic analysis of a solar dish receiver using different nanofluids. Energy 133 (2017)749–760.

[34] Bellos E, Tzivanidis C. Parametric investigation of nanofluids utilization in parabolic trough collectors. Thermal Science and Engineering Progress 2 (2017) 71–79.

[35] Mousavi SV, Sheikholeslami M, Gorjibandpy M, Gerdroodbary MB. The influence of magnetic field on heat transfer of magnetic nanofluid in a sinusoidal double pipe heat exchanger. Chemical

Engineering Research and Design 113 (2016) 112-124.

[36] Khosravi A, Malekan M, Assad MEH. Numerical analysis of magneticfield effects on the heat transfer enhancement in ferrofluids for a parabolic trough solar collector. Renewable Energy 134 (2019) 54-63

[37] Malekan M, Khosravi A, Syri S. Heat transfer modeling of a parabolic trough solar collector with working fluid of Fe_3O_4 and CuO/Therminol 66 nanofluids under magnetic field. Applied Thermal Engineering 163 (2019) 114435.

[38] Bellos E, Tzivanidis C. Assessment of the thermal enhancement methods in parabolic trough collectors. International Journal of Energy and Environmental Engineering 9 (2018) 59–70.

[39] Bellos E, Tzivanidis C, Tsimpoukis D. Enhancing the performance of parabolic trough collectors using nanofluids and turbulators. Renewable and Sustainable Energy Reviews 91 (2018) 358–375.

[40] Bellos E, Tzivanidis C. Enhancing the performance of evacuated and non-evacuated parabolic trough collectors using twisted tape inserts, perforated plate inserts and internally finned absorber. Energies 11 (2018) 1129.

[41] Yang SM, Tao WQ. Heat transfer: 4th Edition. Beijing: Higher Education Press. 2006.

[42] Guo ZY, Li DY, Wang BX. A novel concept for convective heat transfer enhancement. International Journal of Heat and Mass Transfer 41 (1998) 2221-2225. S

[43] Xia ZZ. Augmentation and optimization on heat conduction and convection processes (in Chinese). Doctoral Thesis. Beijing: Tsinghua University, 2001.

[44] Gong JH, Jin W, Xu ZC, Huang BK, Wang J, Wang CL. Numerical study on the uniformity of reflective high concentration photovoltaic system with two-stage reflective concentrator. Solar Energy 199 (2020) 206–213.

[45] Gong JH, Jiang Z, Luo XF, Du B, Wang J, Lund PD. Straight-through all-glass evacuated tube. Solar Energy 201 (2020) 935–945.

[46] Liu SW, Wu YT, Zhang YQ, Du CX, Ma CF. SloTrace simulation and experimental analysis of parabolic trough solar collector. Acta Energiae Solaris Sinica 37 (2016) 3117–3124.

[47] Wendelin T, Dobos A, Lewandowski A. SolTrace: A ray-tracing code for complex solar optical systems. NREL/TP—5500—59163, 2013.

[48] Behar O, Khellaf A, Mohammedi K. A novel parabolic trough solar collector model – validation with experimental data and comparison to Engineering Equation Solver (EES). Energy Conversion and Management 106 (2015) 268–281.

[49] Bellos E, Tzivanidis C. A detailed exergetic analysis of parabolic trough collectors. Energy Conversion and Management 149 (2017) 275–292.